Fine Pointing Control for Optical Communications

Angel A. Portillo*, Gerardo G. Ortiz, Caroline Racho
Jet Propulsion Laboratory
California Institute of Technology
M/S 238-343
4800 Oak Grove Dr.
Pasadena, CA, 91109
(818)354-1471*
Angel.A.Portillo@jpl.nasa.gov*

Abstract— Free-Space Optical Communications requires precise, stable laser pointing to maintain optimal operating conditions. This paper describes the software and hardware implementation of the Fine Pointing Control based on the Optical Communications Demonstrator architecture. The implementation is designed to facilitate system identification of the Fast Steering Mirror mechanism. Models are derived from laboratory testing of two fine steering mirrors that are integrated into the fine tracking loop. Digital controllers are then designed to close the tracking loop using optical feedback. Results of the Fine Pointing Control performance show an improvement of 20% in the jitter rejection bandwidth over previous experiments. A discussion of the computer delay and limited processing bandwidth in this particular implementation are included.

Keywords: Free-Space Optical Communications, Fine Pointing Control.

TABLE OF CONTENTS

1.0 INTRODUCTION
2.0 DEFINITION AND REQUIREMENTS OF FINE POINTING CONTROL
3.0 ATP TEST BED ARCHITECTURE
- 3.1 OPTICAL SETUP
- 3.2 HARDWARE
  - 3.2.1 MODIFIED DALSA CCD
  - 3.2.2 FAST STEERING MIRRORS
- 3.3 REAL-TIME SOFTWARE IMPLEMENTATION
  - 3.3.1 SOFTWARE TIMING

4.0 LABORATORY MEASUREMENTS
- 4.1 SOFTWARE EXECUTION SPEED
- 4.2 CALIBRATION
- 4.3 OPEN LOOP CHARACTERIZATION
- 4.4 CLOSE LOOP PREDICTION
- 4.5 CLOSE LOOP VERIFICATION

5.0 CONCLUSION
6.0 FUTURE WORK

1. INTRODUCTION

This paper describes improvements made to the existing implementation of the JPL patented Optical Communications Demonstrator Acquisition and Fine Tracking. A laboratory test bed has been developed for the purpose of analyzing, implementing, and testing a high bandwidth, precision pointing and tracking system for free-space optical communications. The test bed system has been developed to aid in the implementation of complex algorithms to enable Free-Space optical Communications for Deep-Space scenarios.

The test bed system allows for the implementation of Acquisition, Tracking, and Pointing functions in an effort to obtain an understanding of the discrete components and how each component affects the overall system performance. The integrated system is based on the JPL patented Optical Communications Demonstrator Architecture [1]. The architecture contains a Fine Steering Mechanism, Focal Plane Array Detector, Tracking Processor & Control Electronics, Host Processor for User interfacing and control and two Helium Neon visible lasers. Characterization and validation of the fine pointing control subsystem is facilitated by the test bed and is therefore the focus of this paper. Results presented demonstrate improvement in the rejection bandwidth of the fine pointing control system by upgrading the fine steering mirror with a larger open loop control bandwidth than the legacy fine steering mirror. Improvement is demonstrated from the previous fine steering mirror rejection bandwidth of 60 Hz to 70 Hz after reducing the system sample rate to 1 kHz. Results of two fine steering mirrors are also presented in this paper.

Section 2 defines and describes the existing requirements for fine Pointing Control. Section 3 describes the components of the Acquisition Tracking and Pointing (ATP) test bed. Section 4 describes experiments performed using the test bed. Section 5 discusses results of the experiments. The paper concludes with a summary and approach for future work to achieve less than 1 micro-radian pointing.

2. DEFINITION AND REQUIREMENTS OF FINE POINTING CONTROL

In this paper, Fine Pointing Control is defined as the process required to track a reference "Beacon" laser with a tracking laser on a Focal Plane Array Detector. The pointing

[1] 0-7803-6599-2/01/$10.00 © 2001 IEEE
[2] Updated December 14, 2000

requirements are driven by the allocated margin to handle mis-pointing. Mis-pointing will cause pointing fades at the receiving station. The major factors contributing to mis-pointing are platform vibrations (S/C), the noise of the sensors (NEA), and the spatial quantization (discretization). This paper will focus on improving the vibration rejection bandwidth in order to compensate for S/C vibrations. Improvement is accomplished by upgrading the legacy Fine Steering Mirror (FSM) with new fine steering mirrors with better open loop bandwidth characteristics..

3.0 ATP TEST BED ARCHITECTURE

The Acquisition, Tracking, and Pointing (ATP) test bed is composed of an Optical Setup, Computer Hardware, and Software.

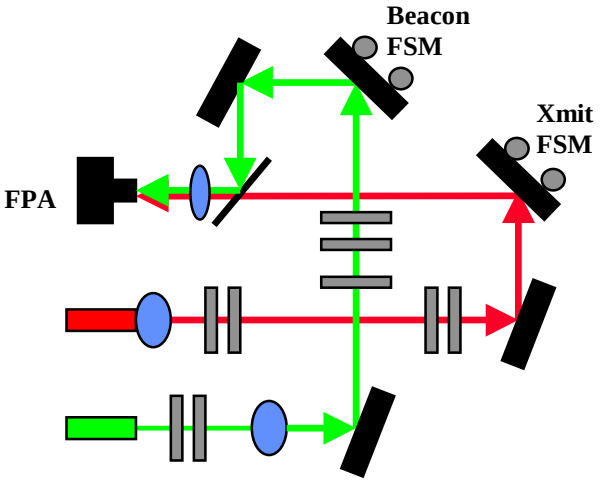

Figure 1 ATP Test Bed Optical Setup

3.1 OPTICAL SETUP

The ATP test bed optical setup is comprised of four optical channels. These are the transmit beam channel, the beacon channel, the focal plane array (FPA) channel and a public demo channel. This optical layout is based on the Optical Communication Demonstrator (OCD) single FPA ATP architecture [1]. The transmit channel contains the down link laser beam (simulated here with a red HeNe), which is pointed towards the ground receiver with the fine-steering mirror. Part of the transmit signal is split in a beam splitter and imaged onto the FPA using the optics in the FPA channel. The beacon channel collects the ground laser beacon (simulated here with a green HeNe). This channel also contains a steering mirror for simulating orbital motion, and ground beacon jitter. The beacon channel is combined with the transmit channel using a beam splitter in order to image it onto the FPA. Both beacon and transmit channels are projected onto a target using the public demo channel. This channel allows for ease of visualization of bean motion on the FPA.

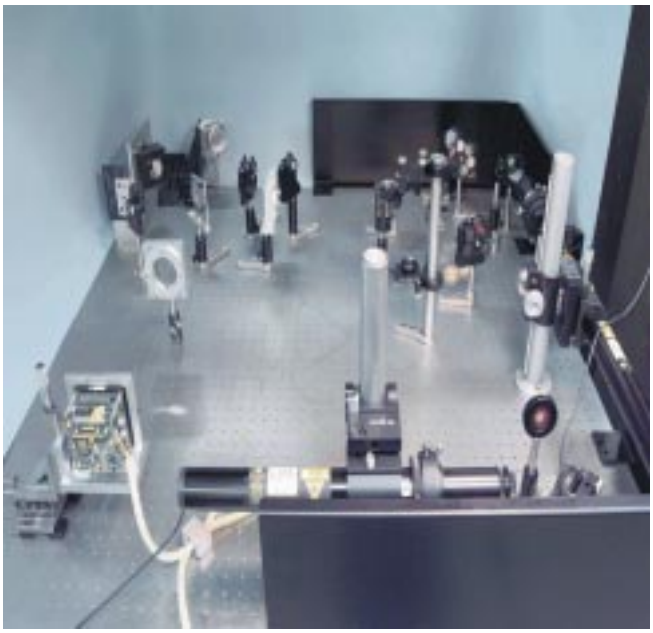

Figure 2 Photograph of the ATP Optical Setup

As a test bed this setup was designed with control parameters to enable characterization of the different components that comprise the ATP system. The testbed allows control of the spot sizes on the FPA, varying from 130 μm to 60 μm. Also, neutral density (ND) filters have been included to control the intensity of the spots on the FPA. The ND filters enable testing of centroid algorithms and characterization of FPAs. The optical setup includes alignment mirrors that facilitate the ability to replace existing components with upgrade components for the purpose of characterization (eg. replacing the FSM or FPA).

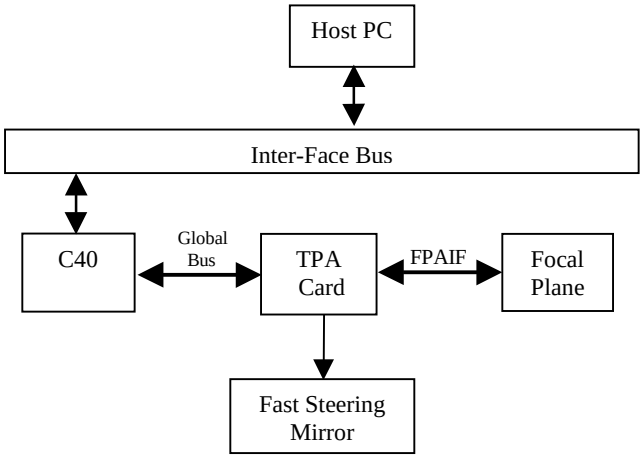

Figure 3 Hardware Description

3.2 HARDWARE

The tracking system hardware consists of a Host PC, a Texas Instruments TMS320C40 Digital Signal Processor (C40), Tracking Processor Electronics, a modified Dalsa CCD, and Left Hand Designs Fast Steering Mirror (FSM),

henceforth denoted as Models FO35 and FO15. Real-time control of the FSM is implemented in the C40 software. The Host PC utilizes a Graphical User Interface to enable user input and data gathering during real-time operation. Communication between the C40 and the Host PC is accomplished via an ISA standard interface to pass data and control parameters from the Host PC to the C40 [2]. A Dalsa CCD Camera that has been modified to facilitate the extraction of sub-windowed images at high frames, minimum 1000 frames per second for these experiments constitutes the FPA. The Fast Steering Mirrors are manufactured by the Left Hand Design Corporation.

3.2.1 MODIFIED DALSA CCD

The FPA is a modified CA-D1 8-bit, single output Dalsa CCD frame transfer camera. The CCD sensor contains 128 x 128, 16um x 16um pixels with a 16 MHz pixel output rate. The Dalsa camera has been modified to facilitate fast sub-window readout to extract two 10x10-pixel windows. Two sub-windows, containing the imaged laser spots of the beacon and transmit laser are read out of the camera at 1000 frames/second to optically close the fine pointing control loop via software control. The maximum frame rate achievable is defined by the speed of execution of the tracking software. A discussion of the tracking software is left for the experimental section of this document. The location of the sub-windows may fall anywhere within the 128x128-pixel area, resulting in a variable time delay to extract the windowed regions of interest. As a result, the time required to obtain the windowed regions of interest varies. Varying window read times are dependent on the size and location of the sub-windows. Typical window read times depend on the time to complete three separate steps. The time to complete each individual step is summed to arrive at the time required for the window read time. The steps are defined as: Scroll Time, Frame Transfer Time, and Window Row Read Time.

3.2.2 FAST STEERING MIRRORS

Two fine steering mirrors were characterized and integrated into the ATP test bed to improve on the legacy General Scanning fast steering mirror [2]. The FO-35 & FO-15 FSMs are two-axis reaction compensated fine steering mirrors manufactured by Left Hand Design Corporation. The FSMs consist of the mirror mechanism, sensor demodulation electronics, current-reference driver, and position-reference servo electronics. The two servo axes are controlled independently via two close loop servos: current-reference and position reference servos. The position servos can operate in one of two modes: base-reference pointing or optical reference pointing. The pointing mode used for fine pointing control is built-in base-referenced position sensor as the feedback sensor [3].

3.3 REAL-TIME SOFTWARE IMPLEMENTATION

The C40 runs the acquisition, tracking, and fine pointing control software. The algorithms implemented assume the following:

1. Constant signal presence for both the Beacon reference and the Transmit laser spot signals on the FPA
2. Neither spot shall fall off the field of view of the FPA
3. Sub-window overlap of the laser spots will not occur
4. Initial angular rate of the beacon is minimal.

The assumptions listed above are valid for laboratory operation of the Optical Tracking System.

The acquisition algorithm implemented extracts a single 10x10-pixel window, one full frame per window, from the FPA in search of a valid beacon centroid signal. The search is implemented by partitioning the 128x128-pixel area into 10x10 sub-windows. A centroid calculation is performed on each sub-window. The centroid algorithm estimates the position of the beacon and reports the result only if a valid beacon signal has been located. A valid beacon signal is defined as a sub-window that contains sufficient intensity based on a predefined value, or intensity threshold, of the

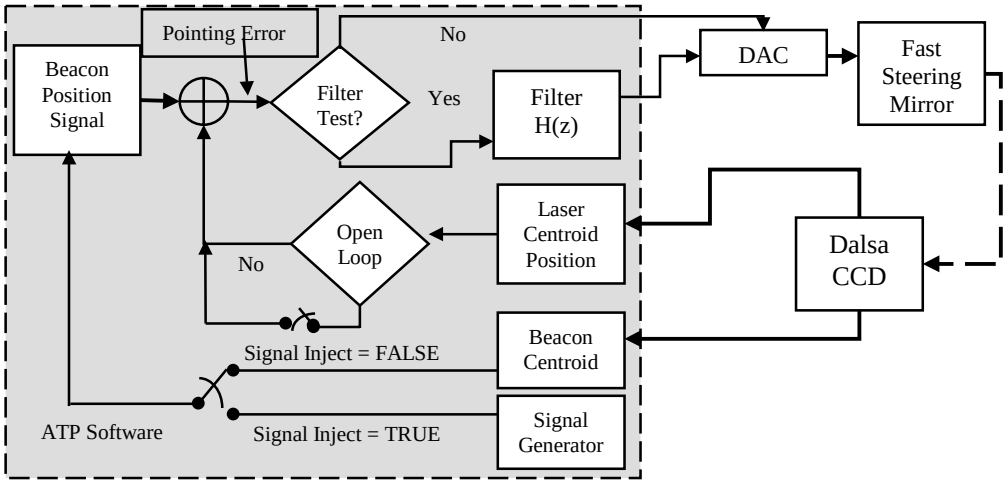

Figure 4 Software Description

sub-window pixel values. The acquisition sequence is completed when all possible sub-windows are processed, recording the window location with the highest intensity value. If the acquisition algorithm locates a valid beacon the software then transitions to a tracking mode, otherwise the process is repeated until a valid beacon signal has been located. During this time the transmit laser spot is placed in a designated area of the FPA so as to avoid confusion between the two distinct laser spots.

Once a valid beacon has been located, the tracking software commences to close the control loop of the steering mirror based on the centroid data, see figure 4. A software state machine executes the transition from acquisition mode to tracking mode. The FSM control loop is optically closed by comparing the beacon position with the transmit laser position with an optical offset added to avoid overlap between the two laser spots. The difference between the two laser spot locations is then used as the error signal into the control loop. The amount of error signal injected into the control loop is initially limited due to the inability of the image tracking software to track laser spots at high angular rates. Once the error signal is at a low level, the full error is then injected into the control loop. The tracking software then attempts to stabilize the line of sight for the transmit laser using optical feedback, as shown if figure 4.

4. Centroid processing
5. Mirror update.

The timing diagram depicts the frame exposure, frame transfer, frame readout, frame processing, and FSM control update. At time equal 0, the exposure of frame zero occurs. At time equal 1 the pixel read out, centroid processing and FSM update occurs of exposure zero occurs, while the exposure of frame 1 occurs in the background. At time equal 2 the response of the controller to frame 0 is scene by the Focal Plane Array during the exposure of frame 2, three samples later, while processing of frame 1 occurs. At time equal 3, exposure of frame 3 occurs, and processing of frame 2 occurs, which contains the information of the response of the loop to the very first frame, while other processing occurs as discussed above. Therefore, optical feedback with this type of architecture will have an inherent 3-sample delay.

Experiments for calibration and analysis of the open loop behavior of the fine pointing control system utilized the software, hardware, and the optical setup discussed above. A digital controller was then designed for the close loop operation of the system.

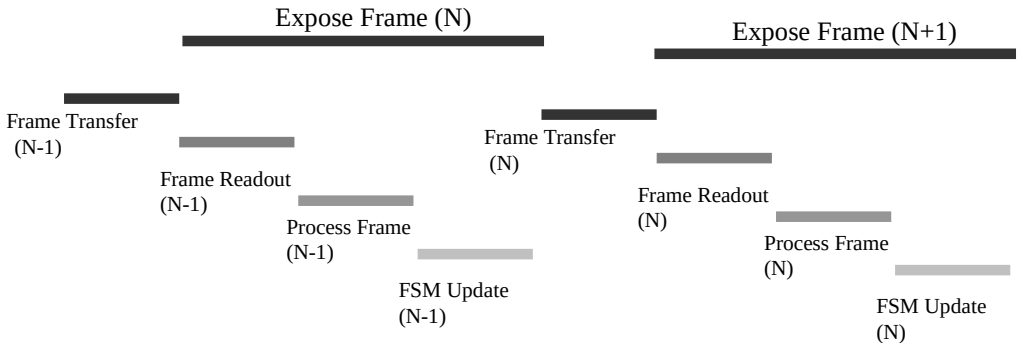

Figure 5 Frame Processing

3.3.1 Software Timing

Real-time operation of the fine pointing control loop is defined by five steps. The timing and execution of each step is critical for optical tracking and pointing control. The amount of time delay induced by digital processing of data used by the feed back path can significantly reduce the performance achievable[4]. Previous experiments demonstrated a 3-sample delay in the optical tracking system digital control loop [2]. The timing, figure 5, of the software versus sample time is shown in figure 5 for three samples of the update loop. The process to update the FSM using optical feedback is a 5-step process:

1. Frame exposure
2. Frame transfer
3. Frame readout

4.0 Laboratory Measurements

For these experiments, the DAC, FSM servo, and mirror are treated as the system plant for the purposes of analyzing the mirror control system. The majority of the system delay comes from the CCD, which acts as the feedback path. Other system components also contribute to the system delay, but are not considered here in detail. The C4x and the C4x software make up the digital filter.

Table 1 Software Benchmark

Process Step	**Time (μS)**
Frame Readout	294.3
Process Frame	362.8
Mirror Update	31.5
Total	688.9

Table 2 Digital Models

FO-15				FO-35			
Horizontal Axis		Vertical Axis		Horizontal Axis		Vertical Axis	
a_i	b_i	a_i	b_i	a_i	b_i	a_i	b_i
-0.44	-0.02275	-0.3704	0.01512	-0.3388	0.01386	-0.306	0.01717
0.3822	-0.08699	0.2288	-0.06355	0.1889	-0.04285	0.1427	-0.1448
0.6433	0.3746	0.629	0.1511	0.7113	0.09865	0.4553	0.568
0.001614	-0.6607	0.007317	-0.623	0.008561	-0.4987	0.004139	-1.129
0.0	1.0	0.0	1.0	0.0	1.0	0.0	1.0

The models, table 2, have –3db bandwidths for the FO-15 Horizontal 331.5 Hz, Vertical Axis 319.8 Hz, FO-35 Horizontal Axis 335.9 Hz, and Vertical Axis 251.5 Hz. Based on the models, closing the feedback loop would result in system instability for both axes for each FSM, FO15 & FO35.

4.1 Software Execution Speed

The software was first benchmarked to determine the maximum update rate possible, table 1. The steps described to update the optical control loop in section 3.3.1 were independently benchmarked. The sum of all the processing steps defines the total time required to perform one update of the digital control loop using optical feedback. The maximum possible frame rate was measured to be approximately 1400 frames per second. The frame rate for these experiments was set to 1000 frames per second to allow for timing variances in the imaging readout. The frame rate selected is a reduction of two from the previous frame rate implemented on OCD [5]. The readout and centroid processing of the pixel data for each sub-window consumes nearly seventy percent of processing time. The centroid algorithm implemented improves upon the legacy algorithm by estimating the value of the background offset from the target laser spots in each separate sub-window.

From table 1, it was determined that the readout time was benchmarked twice as slow, as compared to the legacy system. The legacy system implemented an algorithm to perform both pixel readout and centroid in one step while the new centroid algorithm splits the operation into two steps. The latter algorithm allows for the collection of pixel data to calculate the background offset, the previous algorithm did not.

4.2 Calibration

After selecting a frame rate, the FPA and FSM misalignments and scaling were characterized and corrected for in the ATP software. The FSM to FPA misalignments and scaling were determined by scanning the FSM in each direction independently while consecutively logging centroid values for 5000 data points at discrete steps across the FPA field of view. The mean value of the centroid data was determined and plotted for each discrete step. A linear fit was then performed on the data to find the transformation to correct for the misalignment and scaling.

4.3 Open Loop Characterization

Once the frame rate was selected, i.e. the system sample rate, and the calibration of the FSM to FPA coordinate was completed, tests were performed to characterize the open loop response of the FSM using the ATP software. The ATP software supports open and close loop characterization of the FSM. The procedure to perform open loop characterization is well-documented [2]. Open loop testing was done by injecting a white noise signal with a five pixel peak-to-peak amplitude. The transfer function that includes the digital controller, FSM, FPA, and software delay was then measured. A linear sub-space [6] digital model was then fitted to the data using the System Identification Toolbox from Matlab. The Matlab derived model and the empirical estimate for both the horizontal and the vertical axes are shown in figures 6 & 7 for the FO-15 and figures 14 & 15 for the FO-35 respectively. The digital models for each axes are listed in Table 2, where a given model is defined digitally using the z-transform as:

$$M(z) = \frac{\sum_i a_i z^i}{\sum_j b_j z^j}, i = 0,1,...n;\ j = 0,1,...n \qquad (1)$$

4.4 Close Loop Prediction

Closing the tracking loop without digital compensation would result in instability in both axes for each FSM. Using the z-transform model of the control loop, Proportional-Integral-Derivative (PID) type control controllers were designed to stabilize the FSMs for each axes. The digital version of the Ziegler-Nichols method for PID control design was used to generate the coefficients [7], with the derivative gain set to zero for the FO-15 due to instability issues. The resulting controllers were implemented as IIR digital filters in the software, figures 8 & 9 FO-15 and figures 16 & 17 FO-35. The close loop performance was predicted using a Matlab simulation figures 10 & 11 FO-15 and figures 18 & 19 FO-35. The coefficients for each FSM digital controller are listed table 3.

Table 3 Digital Controllers

FO-15				FO-35			
Horizontal Axis		Vertical Axis		Horizontal Axis		Vertical Axis	
a_i	b_i	a_i	b_i	a_i	b_i	a_i	b_i
-0.05005	-1.0	- 0.1348	-1.0	0.1	0.0	0.25	0.0
0.35	1.0	0.465	1.0	- 0.33	-1.0	- 0.609	-1.0
0.0	0.0	0.0	0.0	0.61	1.0	0.719	1.0

The FO-15 controllers listed in table 3 have the following stability margins and predicted –3dB close loop bandwidths.
Horizontal Stability Margins: 4.9 dB, 70.1^0 ; BW = 196.7 Hz
Vertical Axis Stability Margins: 5.7 dB, 62.4^0, BW = 189.9 Hz

The FO-35 controllers listed in table 3 have the following stability margins and predicted –3dB close loop bandwidths.
Horizontal Stability Margins: 5.7 dB, 62.5^0, BW = 229.5 Hz
Vertical Axis Stability Margins: 5.7dB, 61.1^0, BW = 205.6 Hz

4.5 Close Loop Verification

Close loop performance was verified by injecting digital sine waves at discrete frequencies into the input of the fine pointing control loop. The data was processed to determine the close loop response of each mirrors' axis. During testing, only one axis was tested at a time. Results are presented in, figures 10 & 11 FO-15 and figures 18 & 19 FO-35.

The rejection bandwidth was predicted using Matlab[2,5] and verified to be approximately 60-70 Hz for each FO-15 axis and approximately 70 Hz for each FO-35 axis. The plots are shown in figures 12, 13, 20 & 21, for each mirror respectively.

5.0 Conclusion

In conclusion the close loop and rejection bandwidth have been improved from previous experiments using new FSMs. The improvements are apparent even after reducing the control loop sample rate by a factor of two. Time delay limitations previously measured, have been identified in the digital control loop implementation. Limitations in the control loop and rejection bandwidth are attributed to the limited processing bandwidth that is characteristic to the implemented hardware and software architecture. The processing bandwidth of the ATP system limited the experiments to 1 kHz FSM command rates.

6.0 Future Work

The next steps to improve the implemented tracking loop are to upgrade the FPA with a larger and faster CCD sensor, migrate the existing fine pointing control software to a faster processing platform, and implement inertial sensors to alleviate the need for high beacon update rates. A faster FPA will help to improve on the window readout times. Faster window read times would help to increase the digital control loop command rate. Faster processing platforms would also allow us to increase the speed of execution of the fine pointing control algorithm on the dedicated platform.

Acknowledgments

This work was carried out at the Jet Propulsion Laboratory, California Institute of Technology, under contract with National Aeronautics and Space Administration. Matlab is a registered trademark of the The Mathworks, Inc. The authors would like to thank James Alexander, Steven P. Monacos, Shinhak Lee, and Boris Lurie.

References

[1] T. Yan, M. Jeganathan, J. R. Lesh, "Progress on the Development of the Optical Communications Demonstrator", *Free Space Laser Communication Technologies IX, SPIE Proceedings*, February 1997.

[2] C. Racho and A. Portillo, "Characterization and Design of Digital Pointing Subsystem for Optical Communications", *Free Space Laser Communication Technologies XI,* Proc. SPIE, Vol. 3615, 1999.

[3] Left Hand Design Corporation, "FSM Operators Manual", *Revision Initial,* September 8, 1998.

[4] B. Lurie, "Feedback limits in the steering mirror loops caused by computer delay", *JPL Internal Memorandum*, September 2000.

[5] M. Jeganathan, et. al., "Lessons Learnt from the Optical Communications Demonstrator", *Free Space Laser Communication Technologies XI,* Proc. SPIE, Vol. 3615, 1999.

[6]P. van Overschee, B. De Moor, "Subspace Identification for Linear Systems: Theory, Implementation, Applications", *Kluwer Academic Publishers*, Norwell, MA1996.

[7] C. L. Philips, H. T. Nagle, "Digital System Control: Analysis and Design", 2nd Edition, *Prentice Hall*, Englewood Cliffs, New Jersey, 1990.

Angel A. Portillo *graduated from the University of Texas at El Paso in 1995 with a B.S. in Computer Engineering. He received an M.S. degree in Computer Engineering from The University of Texas at El Paso in 1997, while assisting in research activities in the area of Image Processing. He is currently a member of the technical staff of the Digital Signal Processing Research Group of the Communications Systems and Research Section at the Jet Propulsion Laboratory in Pasadena, California. His research interests include, computer vision, image segmentation techniques, real-time control systems, and computer architecture.*

Gerry G. Ortiz the B.S.E.E. ('86) degree from UCLA and the M.S. ('93) and Ph. D. ('97) degrees in Opto-electronics from the University of New Mexico, Albuquerque, NM. After UCLA, he worked at the Jet Propulsion Laboratory developing millimeter-wave cryogenically-cooled Low Noise Receivers for JPL's Deep Space Network. In 1991, he was awarded a NASA Doctoral Fellowship to pursue graduate work at the University of New Mexico. While at UNM he focused on developing high-speed optical communications. His thesis work was the successful development of a wavelength division multiplexed (WDM) vertical-cavity surface-emitting laser (VCSEL) array monolithically integrated with wavelength matched WDM resonant-cavity enhanced photo-detectors. This yielded an opto-electronic communication fabric to enable over 20 channels of high-speed computer backbone inter-connects from a simple fabrication technique. In 1997 he joined the Free-Space Optical Communication Group at JPL. He is currently active in many aspects of the free-space optical link: system engineering, acquisition, tracking and pointing technology, efficient space lasers, and ultra-sensitive receiver development. He has just completed design of an ultra-sensitive large-area opto-electronic receiver for Mars missions and is currently Cognizant Engineer for the Acquisition, Tracking and Pointing Test-bed development for deep space missions and technology research. He has authored over 20 refereed papers, articles and conference presentations.

Caroline Racho received her B.A. in Applied Mathematics from the University of California at Berkeley in 1986. She received her M.S. in Electrical Engineering from the University of Southern California in 1992. She is currently at the Jet Propulsion Laboratory, California where she is a system engineer in the Wireless Communications Group. Her current area of interest is in digital signal processing in communication systems.

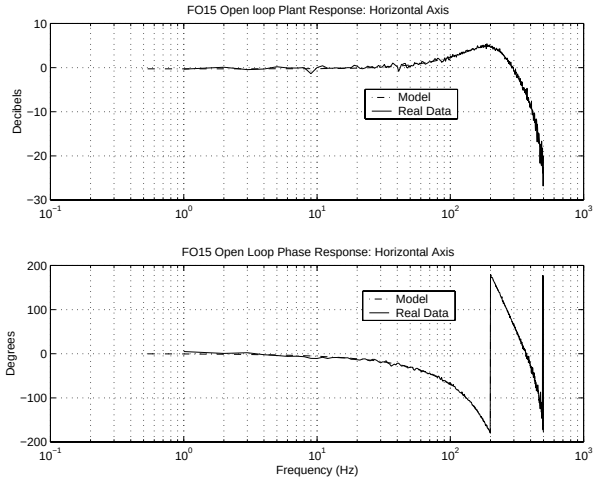

Figure 6 FO15 Open Loop Response – Horizontal Axis

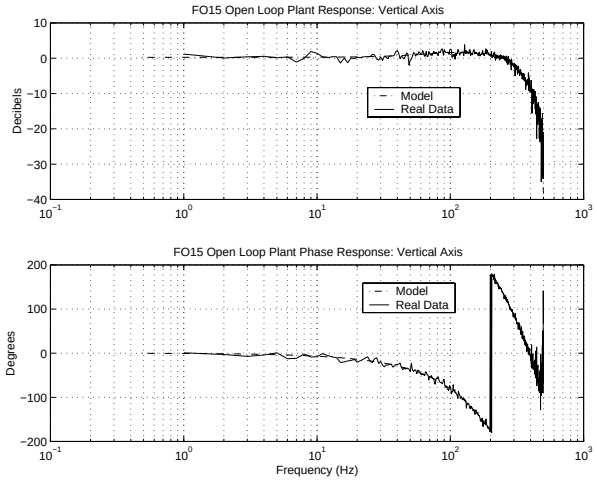

Figure 7 FO15 Open Loop Response – Vertical Axis

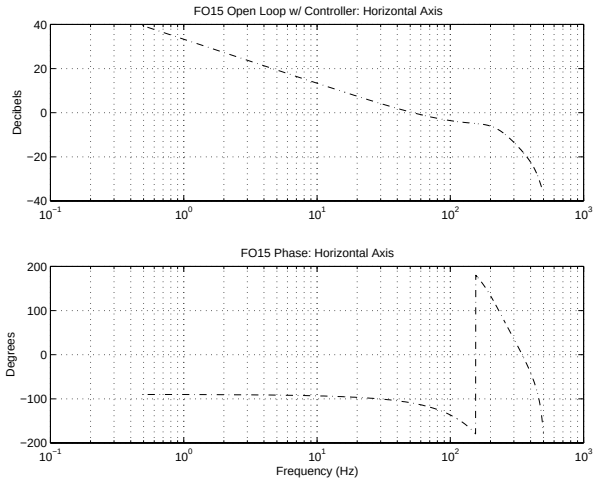

Figure 8 FO15 w/ Controller – Horizontal Axis

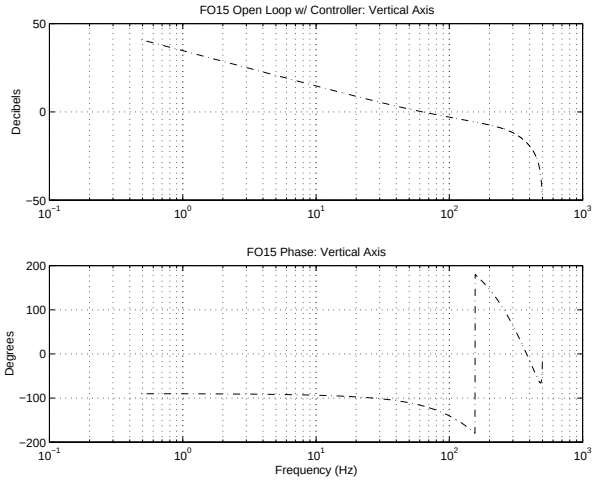

Figure 9 FO15 w/ Controller – Vertical Axis

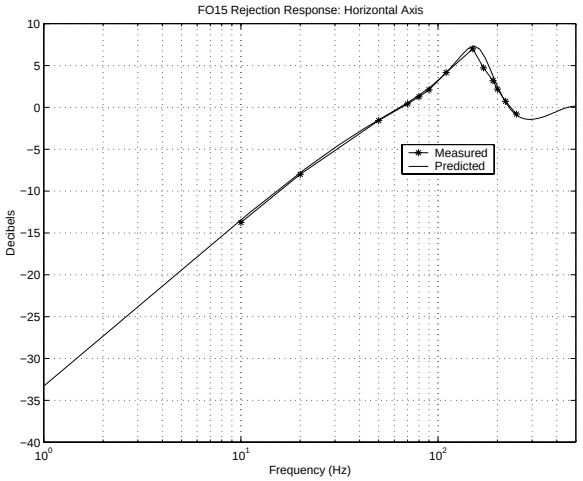

Figure 12 FO15 Rejection Response – Horizontal Axis

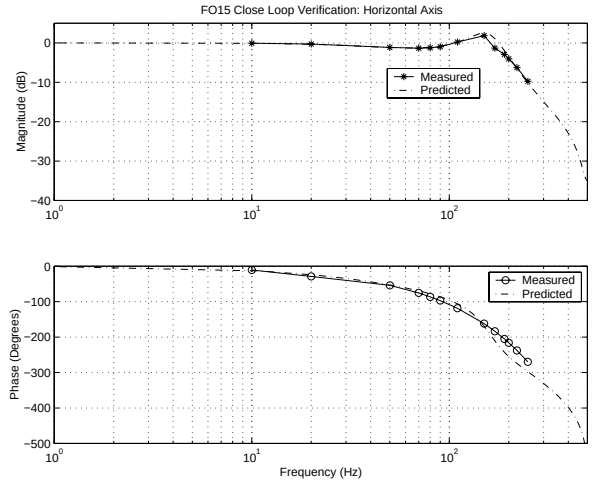

Figure 10 FO15 Close Loop – Horizontal Axis

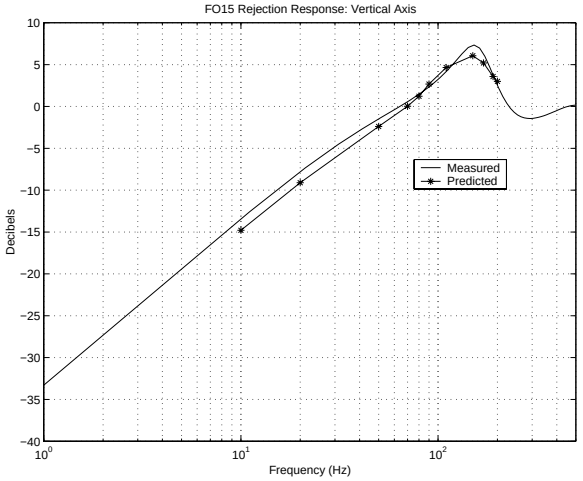

Figure 13 FO15 Rejection Response – Vertical Axis

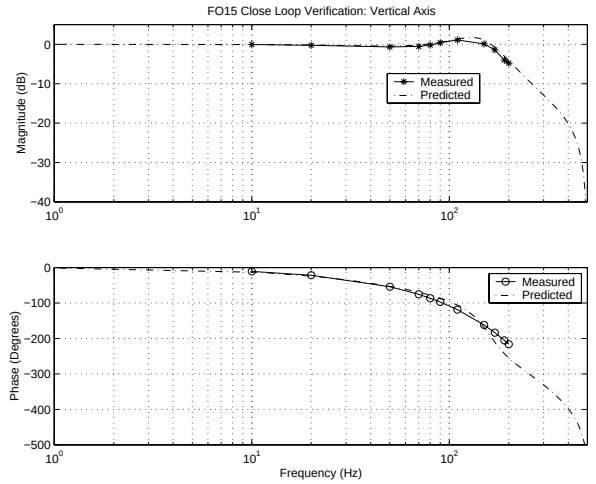

Figure 11 FO15 Close Loop – Vertical Axis

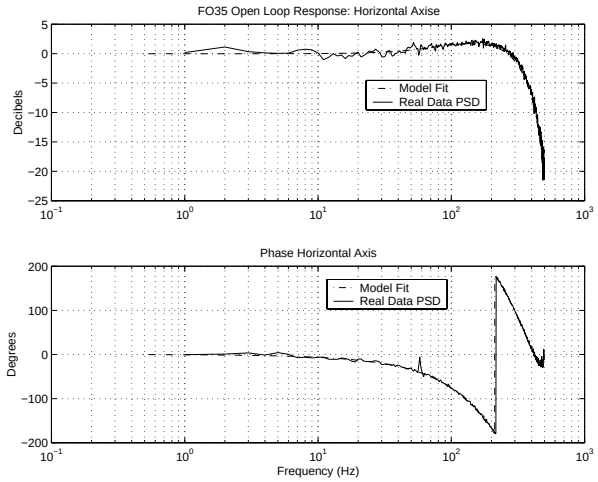

Figure 14 Open Loop Response – Horizontal Axis

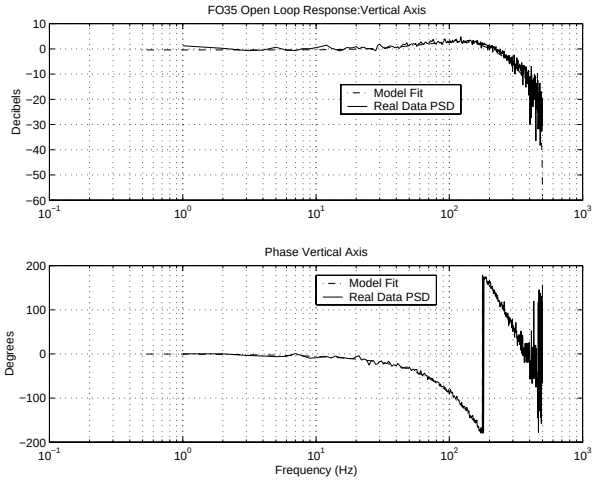

Figure 15 Open Loop Response – Vertical Axis

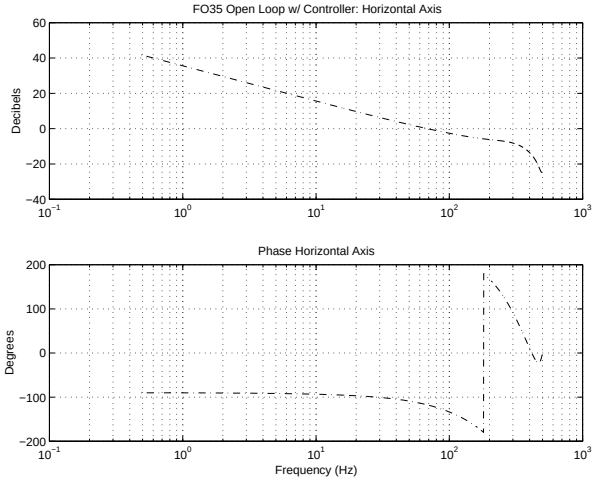

Figure 16 FO35 Open Loop w/ Controller – Horizontal Axis

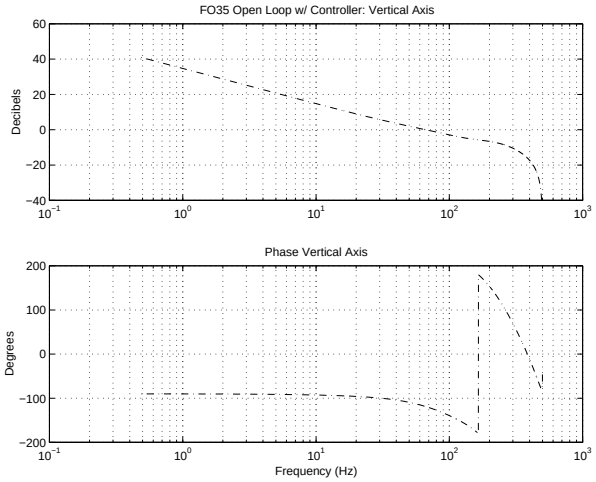

Figure 17 FO35 Open Loop w/ Controller – Vertical Axis

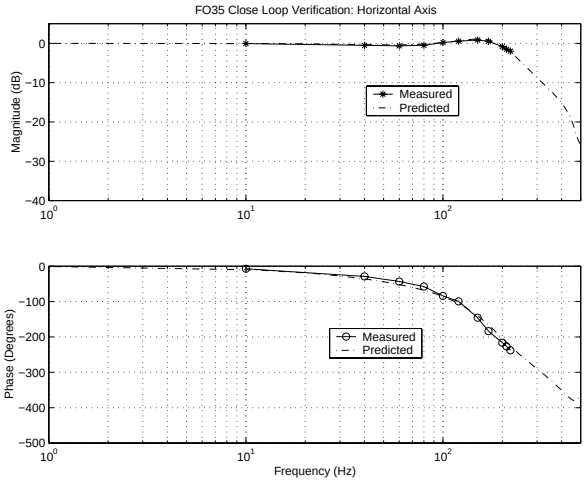

Figure 18 FO35 Close Loop – Horizontal Axis

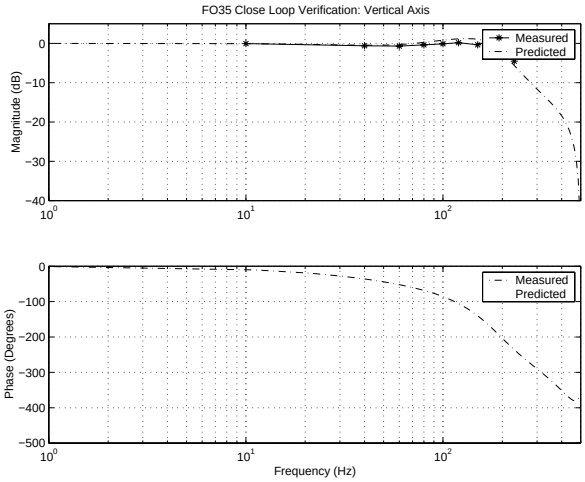

Figure 19 FO35 Close Loop – Vertical Axis

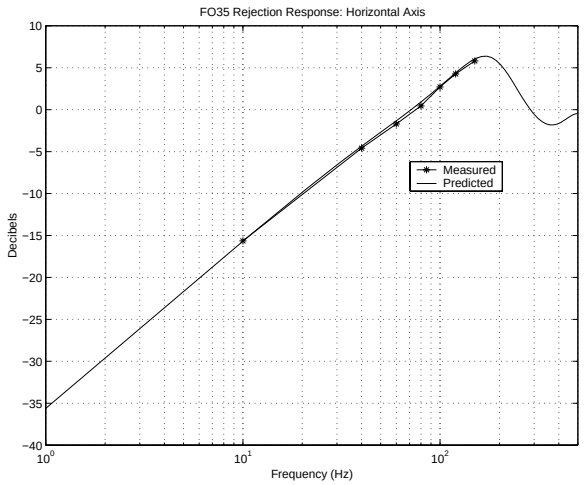

Figure 20 FO35 Rejection Response – Horizontal Axis

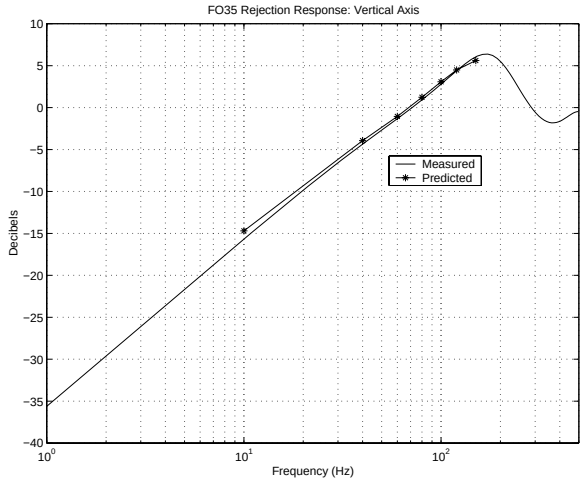

Figure 21 FO35 Rejection Response – Vertical Axis